DOI: 10.1002/ejic.200900216

Synthesis, Structures, and Photophysical Properties of Two Organostannoxanes from a Novel Acrylic Acid Derived from Phenothiazine

Dongmei Li,[a] Rentao Hu,[a] Wen Zhou,[a] Pingping Sun,[a] Yuhe Kan,[b] Yupeng Tian,*[a,c,d] Hongping Zhou,*[a] Jieying Wu,[a] Xutang Tao,[c] and Minhua Jiang[c]

Keywords: Tin / Photophysics / Structure–activity relationship / Charge transfer

(*E*)-3-(10-ethylphenothiazine-3-yl)acrylic acid (LCOOH) was synthesized. LCOOH reacted with $Ph_3Sn(OH)$ and nBu_2SnO to afford Ph_3SnO_2CL (**1**) and $\{[nBu_2SnO_2CL]_2O\}_2$ (**2**), respectively. The structures of all the compounds were solved by single-crystal X-ray diffraction. Compounds **1** and **2** present discrete and ladder frameworks, respectively. The one-photon absorption and excited fluorescence, and two-photon excited fluorescence spectra of all the compounds were systematically investigated. The results show that the two organostannoxanes exhibit much more enhanced two-photon absorption properties than LCOOH. TDDFT computational studies have been performed to elucidate the electronic structures of the ground state of LCOOH.

Introduction

Since the 1990s, increasing attention has been devoted to two-photon absorption (TPA) based applications in photonic and biophotonic areas, such as three-dimensional optical data storage and microfabrication,[1] power limiting,[2] up-conversion lasing,[3] three-dimensional fluorescence imaging,[4] and photodynamic therapy.[5] Extensive efforts have been concentrated on the synthesis of various chromophores with large TPA cross-sections (δ), such as polymers,[6] small organic molecules,[7] semiconductor or metal nanoparticles[8] and organometallic compounds.[9] In comparison with small organic molecules, organometallic compounds are expected to show better secondary properties, namely physical, thermal, and mechanical properties that are important to material processing and device fabrication, and should not be neglected and must be addressed in parallel with continuing efforts to enhance the effective δ values.

In recent years, there has been considerable interest in organotin compounds, for some of them are biologically active or have been used as reagents or catalysts in organic reactions.[10] Furthermore, a surprisingly large structural diversity can be achieved by relatively simple synthetic variations from organotin compounds. Hydrolyzed products (oxides, hydroxides, and oxohydroxides) for the hydrolytic reactions of organotin halides serve as precursors for reactions with various reagents, such as carboxylic, phosphonic, phosphinic, or sulfonic acids. Several novel cluster types such as ladder,[11] drum,[12] *O*-capped,[13] cube,[14] butterfly,[15] triply- and doubly bridged ladders,[16,17] have been assembled and structurally characterized, although there is still no systematic investigation of the TPA properties of organotin compounds, one that includes the results from one-photon absorption (OPA), one-photon excited fluorescence (OPEF), and two-photon excited fluorescence (TPEF) spectroscopy and the crystal structure determination.

Our efforts have been directed towards the search for optimized molecular structures having large TPA cross-sections. Carboxylic acid is a strong acceptor (A), and therefore a general motif of the type D–π–A may efficiently be constructed with a donor (D) group. Phenothiazine (ptz) was chosen as the D group, for its derivatives are well known as dyes, antioxidants, and pharmaceuticals.[18,19] The electron-rich ptz ring has two important properties that make it ideal: (i) ptz is a strong electron donor because of its low oxidation potential ($E_{1/2}$ = +0.59 V in acetonitrile vs. SCE),[20,21] (ii) unlike carbazole, the nonplanar ptz ring structure restricts π-stacking aggregation, which prevents the detrimental pure singlet exciton recombination process.[22] In such cases, the vinyl unit was used as the π

[a] Department of Chemistry, Key Laboratory of Functional Inorganic Materials Chemistry of Anhui Province, Anhui University,
Hefei 230039, P. R. China
E-mail: yptian@ahu.edu.cn
zhpzhp@263.net
[b] Department of Chemistry, Jiangsu Province Key Laboratory for Chemistry of Low-Dimensional Materials, Huaiyin Teachers College,
Huai an 223001, P. R. China
[c] State Key Laboratory of Crystal Materials, Shandong University,
Jinan 250100, P. R. China
[d] State Key Laboratory of Coordination Chemistry, Nanjing University,
Nanjing 210093, P. R. China

Supporting information for this article is available on the WWW under http://dx.doi.org/10.1002/ejic.200900216.

bridge.[1] Consequently, (*E*)-3-(10-ethylphenothia-zine-3-yl)-acrylic acid (LCOOH) was synthesized. LCOOH reacted with $Ph_3Sn(OH)$ and nBu_2SnO to afford the mono- and tetranuclear products, respectively. All three compounds were fully characterized, and structure-property relationships have been established. Time-dependent density functional theory (TDDFT) computational studies have been performed to elucidate the electronic structures of the ground state of LCOOH.

Results and Discussion

Preparation of the Compounds

The synthetic routes for all the compounds are shown in Scheme 1. 10-Ethylphenothiazine-3-carbaldehyde[23] reacted with $CH_2(COOH)_2$ to afford LCOOH as the pure *E* compound. The ^1H NMR spectrum of LCOOH in $CDCl_3$ shows doublets at δ = 6.30 (J = 16.06 Hz) and 7.66 (J = 16.06 Hz) ppm for the vinyl protons. LCOOH reacted with $Ph_3Sn(OH)$ and nBu_2SnO to afford the mono- and tetranuclear products **1** and **2**, respectively. The IR spectra show that $\nu_{C=O}$ bands appear at 1686, 1640, and 1638 cm^{-1} for LCOOH, **1**, and **2**, respectively. The solubility of the tetranuclear product **2** in many polar and nonpolar solvents is much better than that of LCOOH. The structures were solved by single-crystal X-ray diffraction; **1** and **2** show discrete and ladder frameworks, respectively. The solution ^{119}Sn NMR spectrum of **1** (see Experimental Section) exhibits a single peak at δ = –115.6 ppm, which is consistent with a monomeric structure in solution.[24–27] The solution ^{119}Sn NMR spectrum of **2** shows two peaks at δ = –202.4 and –219.2 ppm, which reveals that the tetrameric structures found in the solid state (vide infra) are retained in solution.[24–27] The thermogravimetric analysis (TGA) show that **1** and **2** have a higher thermal stability than LCOOH.

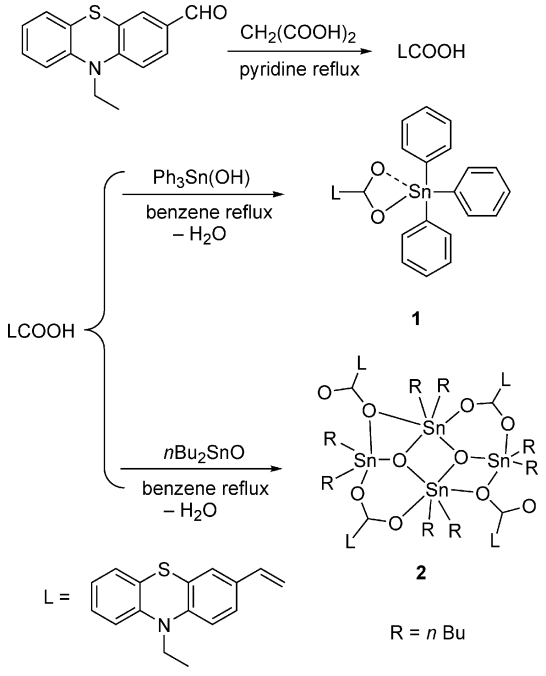

Scheme 1. Synthesis of the three compounds.

Description of the Crystal Structures

$C_{17}H_{15}NO_2S$ (LCOOH)

LCOOH crystallizes in the monoclinic space group $P2_1/c$. Figure 1A shows an ORTEP plot of the molecule with the atom numbering scheme. The molecular structure shows that two LCOOH molecules form a dimer through π···π stacking between the phenyl rings of the ptz units, with a centroid–centroid distance of 3.775 Å and a dihedral angle of 1.88°.[28] The configurations of the two molecules are similar; the first ptz unit is folded about the S1–N1 axis with a dihedral angle of 143.00°, whereas the second ptz unit is folded about the S2–N2 axis with a dihedral angle of 145.69°. Bond lengths and angles are summarized in Table 1. As shown in Figure 1B, short S···S contacts occur between two kinds of molecules, which lead to a 1D chain structure along the *c* axis [d(S1A···S2B) = 3.570 Å].[29] The 1D chains interact with each other through two kinds of O–H···O interactions to form a 3D structure (Figure 1C).

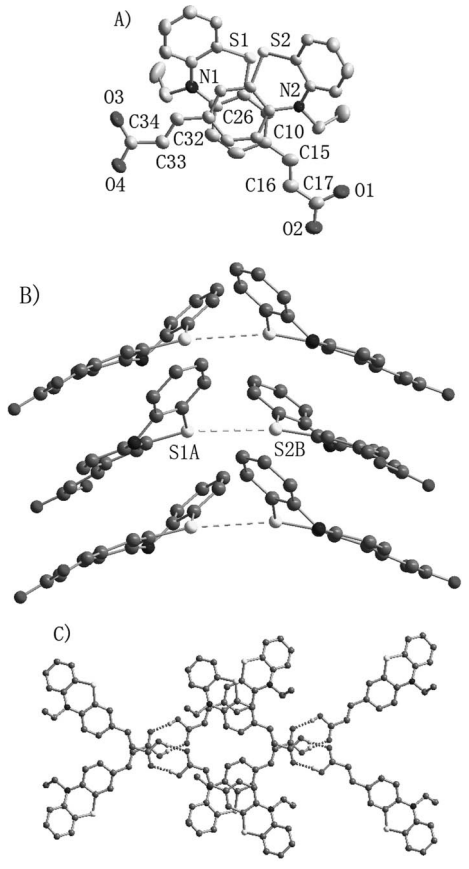

Figure 1. (A) ORTEP structure of LCOOH with the atom labeling scheme; all hydrogen atoms are omitted for clarity. (B) 1D chains along the *c* axis formed by S···S contacts. (C) 1D chains interact with each other through H bonds (O–H···O) formed by adjacent molecules to generate a 3D structure.

H bonds are formed between two neighboring molecules with the same configurations [*d*(O2A···O1B) = 2.834 Å, ∠(O1B–H1B···O2A) = 170.96°; *d*(O4A···O3C) = 2.615 Å, ∠(O4C···H3A–O3A) = 163.39°].[30]

Table 1. Selected bond lengths [Å] and angles [°].

Compound	Bond lengths		Bond angles	
LCOOH	C10–C15	1.467(5)	C16–C15–C10	127.2(4)
	C15–C16	1.322(5)	C15–C16–C17	124.1(4)
	C16–C17	1.455(5)	O1–C17–C16	117.5(4)
	C17–O2	1.240(5)	O2–C17–O1	122.9(4)
	C17–O1	1.285(5)	O2–C17–C16	119.6(4)
	C26–C32	1.459(5)	C33–C32–C26	126.9(4)
	C33–C32	1.309(5)	C32–C33–C34	126.2(5)
	C34–C33	1.449(6)	O3–C34–C33	117.9(4)
	C34–O3	1.293(5)	O4–C34–C33	119.3(4)
	C34–O4	1.235(5)	O4–C34–O3	122.8(4)
1	Sn1–O1	2.070(2)	O2–C17–O1	120.9(3)
	Sn1–O2	2.659(2)	O1–Sn1–O2	53.83 (2)
2	Sn4–O020	2.040(5)	O020–Sn4–O013	76.9(2)
	Sn4–O013	2.170(5)	O020–Sn4–O5	91.5(2)
	Sn4–O5	2.292(7)	O013–Sn4–O5	167.2(2)
	Sn4–O8	2.726(7)	O013–Sn4–O8	63.6 (2)
	Sn3–O013	1.982(6)	O013–Sn3–O8	78.2(2)
	Sn3–O8	2.174(6)	O013–Sn3–O4	88.1(2)
	Sn3–O4	2.256(6)	O8–Sn3–O4	166.3(2)
	Sn2–O013	2.069(5)	O013–Sn2–O020	76.3(2)
	Sn2–O020	2.171(6)	O013–Sn2–O3	90.9(2)
	Sn2–O3	2.277(7)	O020–Sn2–O3	166.2(2)
	Sn2–O2	2.769(6)	O2–Sn2–O3	127.8(2)
	Sn1–O020	2.008(6)	O020–Sn1–O2	79.7(2)
	Sn1–O2	2.170(6)	O020–Sn1–O6	87.7(2)
	Sn1–O6	2.236(6)	O2–Sn1–O6	166.9(2)
H bond	C65B···O1A	3.533	C65B–H65B···O1A	162.12
	C70B···O1A	3.514	C70B–H70B···O1A	175.80
	C10A···O7B	3.341	C10A–H10A···O7B	170.11
	C16A···O7B	3.422	C16A–H16A···O7B	171.84

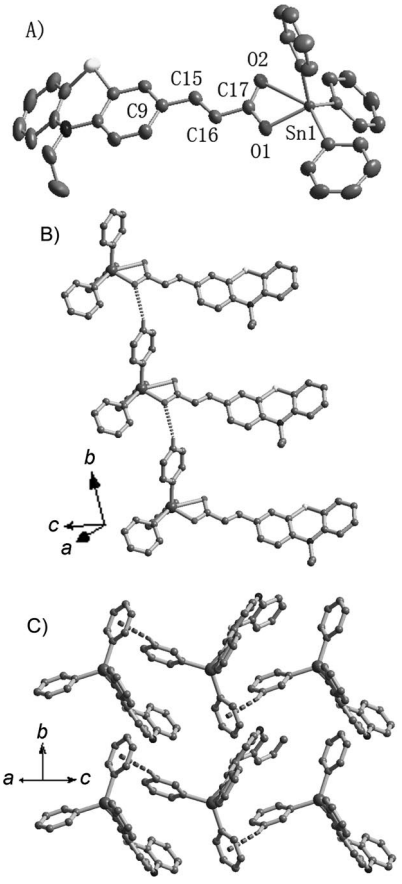

Figure 2. (A) ORTEP structure of **1** with the atom labeling scheme; all hydrogen atoms are omitted for clarity. (B) Intermolecular H bonds (C–H···O) between the molecules in the 1D chains. (C) 1D chains interact with each other through C–H···π stacking interactions formed by adjacent molecules to generate a 3D structure.

Ph_3SnO_2CL (1)

Compound **1** crystallizes in the monoclinic space group $P2_1/c$ with the formula [Ph_3SnO_2CL]. Figure 2A shows an ORTEP plot of the molecule with the atom labeling scheme. Compound **1** has a discrete structure;[24–27] the geometry around the tin atom can be described as capped tetrahedral. Two types of Sn–O bond lengths are found: Sn–O1 2.070(2) and Sn–O2 2.659(3) Å.[31] The ptz unit is folded about the S1–N1 axis with a dihedral angle of 151.64°, which indicates a smaller torsion of the ptz unit in **1** relative to that in the free ligand. This may facilitate π-electron delocalization in **1**. Adjacent molecules interact with each other through H bonds to form a 1D chain structure along the *b* axis (Figure 2B). The oxygen atom of the ligand is the H-bonding acceptor, and the H(C) donor is from the phenyl substituent on the tin atom. The C···O distance is 3.533 Å and the C–H···O angle is 144.520°.[32] Further intermolecular C–H···π interactions between the phenyl substituents on the tin atoms from neighboring chains lead to a 3D structure (Figure 2C); the C–H···π separation is 2.999 Å.[33]

[{[nBu_2SnO_2CL]$_2$O}$_2$] (2)

Compound **2** crystallizes in the orthorhombic space group $Pna2_1$ with the formula {[nBu$_2$SnO$_2$CL]$_2$O}$_2$. Figure 3A shows an ORTEP plot of the molecule with the atom numbering scheme. The crystal structure of **2** shows a ladder framework.[24–27] The centrosymmetric structure features a central $Bu_4Sn_2O_2$ core to which two Bu_2Sn entities are linked with the result that the O013 and O020 atoms are three coordinate. The bond lengths and angles for the central Sn_2O_2 core are given in Table 1. The ligand is involved in both anisobidentate chelating [Sn1–O2 2.008(6), Sn2–O2 2.171(6), Sn3–O8 2.174(6), and Sn4–O8 2.726(7) Å] as well as isobidentate bridging coordination modes (Sn1–O6 2.236(6), Sn4–O5 2.292(7), Sn2–O3 2.277(7), and Sn3–O4 2.256(6) Å; these values fall in the typical Sn–O bond length range[31]). Each of the independent tin atoms in the structure exhibits a distorted trigonal bipyramidal geometry, with a C_2O trigonal plane and axial positions that are occupied by oxygen atoms. As shown in Figure 3B and Table 1, four types of intermolecular H bonds between adjacent molecules lead to a 1D chain structure.[32] The ptz unit is also involved in C–H···π interactions with CH protons of the ptz unit from a neighboring mole-

cule; the C–H···π separation is 2.781 Å (Figure 3C).[33] Such further intermolecular C–H···π interactions between adjacent 1D chains generate a 3D structure.

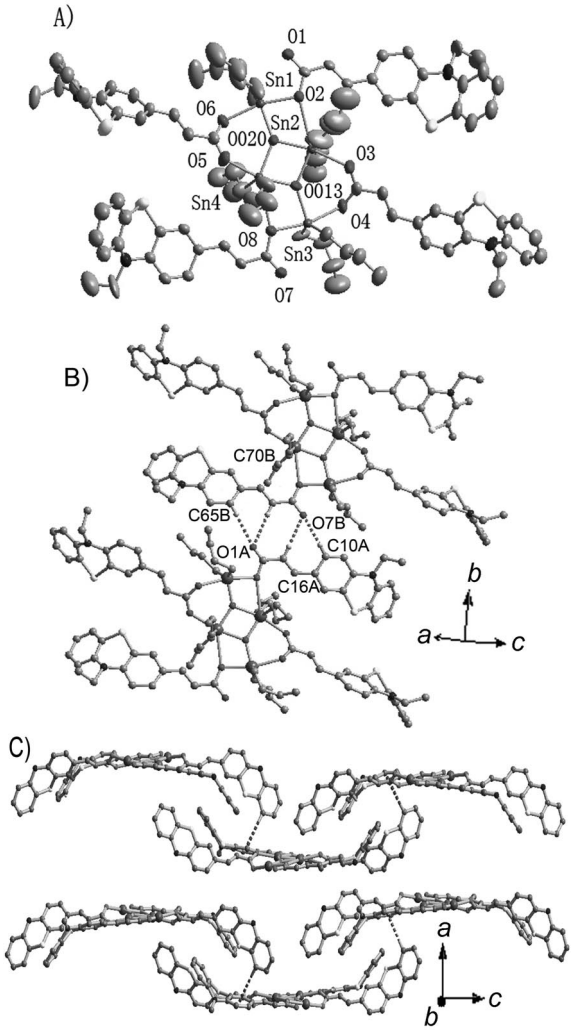

Figure 3. (A) ORTEP structure of **2** with atom labeling scheme; all hydrogen atoms are omitted for clarity. (B) Intermolecular H bonds (C–H···O) between molecules in the 1D chains. (C) 1D chains interact with each other through the C–H···π stacking interactions between adjacent molecules to generate a 3D structure.

Computational Studies

TDDFT computational studies were performed to elucidate the electronic structures of the ground state of LCOOH. For this purpose, the model compound LCOOH′ was used instead of LCOOH, in which the ethyl group on ptz is replaced by a methyl group. Optimizations were carried out with B3LYP [6-31G(d)] without any symmetry restraints, and the TDDFT {B3LYP [6-31G(d)]} calculations were performed on the optimized structure.[34] All calculations, including optimizations and TDDFT, were performed with the G03 software.[35] In the calculation of the optical absorption spectrum, the 25 lowest spin-allowed singlet–singlet transitions, up to an energy of about 5 eV, were taken into account.[36] The optimized structure shows that the ptz unit is folded about the S–N axis with a dihedral angle of 140°. This value is very similar to the experimental results (143.00 and 145.69°). The calculated C10–C15 distance [1.459 Å] is the same as the experimental C26–C32 bond length [1.459(5) Å]. The simulated C15–C16 and C16–C17 bond lengths [1.350 and 1.470 Å, respectively] are slightly longer than the corresponding experimental data (Table 1). The O–C–O bond angle (122.08°) is about 0.82 and 0.72° smaller than the experimental bond angels for O2–C17–O1 and O4–C34–O3, respectively. Generally, our calculated geometrical parameters for the ground state are in agreement with experimental X-ray data. The spatial plots of selected TDDFT frontier molecular orbitals of LCOOH′ are shown in Figure 4. The energies of the frontier orbitals in LCOOH′ and the percentage compositions of these frontier orbitals are listed in Table 2.

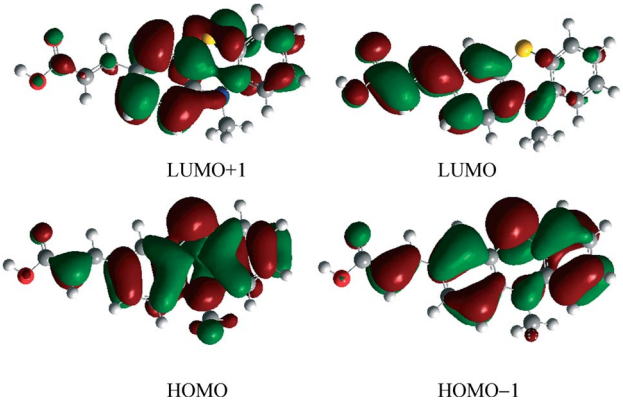

Figure 4. DFT computed frontier orbitals of LCOOH′ obtained at the B3LYP level.

Table 2. Selected low-lying singlet (S_n) excited states computed by the TDDFT method, with the orbitals involved (OI) in the excitations. Transition coefficient (T_c), excitation energies (in eV and nm), and oscillator strengths (f) for LCOOH′.

Compound	S_n	Character	OI[b]	T_c[c]	Excitation energy [eV/nm]	f [d]
LCOOH′	S_1	ICT	H→L	0.66	3.07/403.56	0.17
	S_3	$\pi\pi^*_{(D)}$[a]	H→L+1	0.48	4.12/300.93	0.36
		ICT	H-1→L	0.35		

[a] $\pi\pi^*_{(D)}$ ($\pi\rightarrow\pi^*$) transition assigned from the D group. [b] H (HOMO), L (LUMO). [c] Excitations with transition coefficients less than 0.35 are not shown. [d] Only the singlet excited state with $f > 0.15$ are listed.

The HOMO and HOMO–1 of LCOOH′ consist mainly of the π orbitals localized on ptz (denoted as π_D). The LUMO orbital is a π* orbital localized on the CH=CH–COOH unit ($\pi^*_{CH=CH-COOH}$). The LUMO+1 consists of π* orbitals localized on ptz (denoted as π^*_D). The lowest-energy excitation band of LCOOH′ is assigned as the intramolecular charge transfer (ICT) transition [$\pi_D\rightarrow\pi^*_{CH=CH-COOH}$] because of the HOMO→LUMO transition. The remaining one band (λ_{max} = 301 nm, f = 0.36) is assigned mainly to a $\pi_D\rightarrow\pi^*_D$ transition as a result of the

HOMO→LUMO+1 transition with some contribution from an ICT transition [$\pi_D \rightarrow \pi^*_{CH=CH-COOH}$, HOMO–1→LUMO].

Luminescence Properties

One-Photon Absorption (OPA) and Excited Fluorescence (OPEF) Spectroscopy

The photophysical data of all the compounds are summarized in Table 3. The OPA and OPEF spectra of LCOOH in four organic solvents and of all the compounds in CH_2Cl_2 are shown in Figures 5 and 6, respectively.

Table 3. Photophysical data of LCOOH, **1**, and **2**.

Compound	Solvent	λ^{ab}[a]	λ^{em}[b]	λ[c]	λ^{TP}[d]	Φ[e]	δ[f]
LCOOH	hexane	290,383	491	574		0.71	
	benzene	284,389	525			0.86	
	CH_2Cl_2	293,391	545		565	0.49	36
	dmf	294,392	554			0.60	
1	CH_2Cl_2	290,363	537	564	555	0.37	53
2	CH_2Cl_2	302,401	557	560	557	0.20	223

[a] Peak position of OPA in nm. [b] Peak position of OPEF in nm. [c] The solid-state emission maxima in nm. [d] Peak position of TPEF in nm. [e] The fluorescence quantum yield. [f] TPA cross-section in GM.

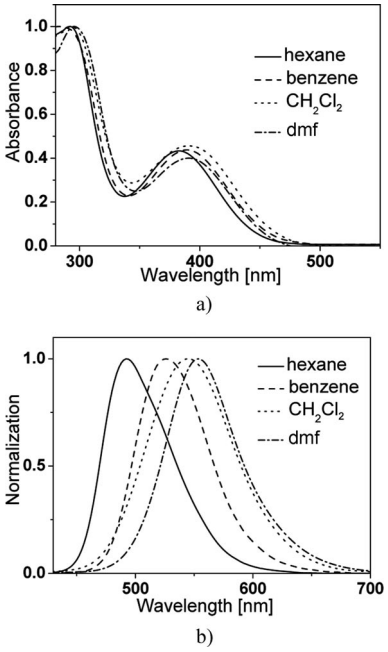

Figure 5. (a) OPA and (b) OPEF spectra of LCOOH in four organic solvents with a concentration of 1×10^{-5} M.

Solvatochromism

Generally, the OPA spectra of LCOOH feature an intense absorption band between 284 and 294 nm and a moderately intense absorption in the range 383–392 nm in all the solvents (Figure 5a). Since the number of bands and their intensities correlate well with the calculated spectra, the calculated assignments for electronic transitions (addressed earlier) appear reasonable. From Figure 5 and Table 3, weak solvatochromism was observed in the absorption bands, which indicates fairly small dipole moments and a comparable ground-state electronic structure in LCOOH.

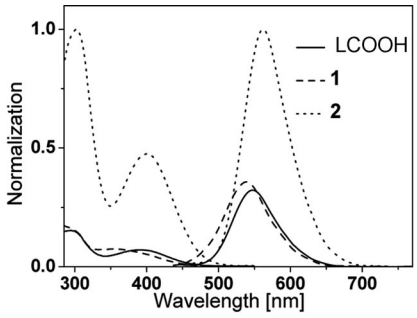

Figure 6. OPA (left) and OPEF (right) spectra of LCOOH, **1**, and **2** in CH_2Cl_2 ($c = 1 \times 10^{-5}$ M).

The OPEF spectra of LCOOH exhibit one strong emission band in the range 491–554 nm, which shows strong solvatochromism. With increasing polarity of the solvent, the emission maxima (λ_{max}^{em}) show remarkable bathochromic shifts. As shown in Figure 5b, λ_{max}^{em} is located at 491 nm in hexane and is redshifted to 554 nm in dmf. These results suggest that the molecular polarity of the fluorescent excited state of LCOOH must be larger than that of the ground state, as the enhanced dipole–dipole interactions caused by increasing the polarity of solute and/or solvent will lead to a more significant energy level decrease for the excited state.

Comparison of the Data for Organostannoxanes with that of the Ligand

The observation of similar absorption bands for the organotin compounds and LCOOH suggests their assignments as the metal-perturbed ICT of the ligand (Table 3 and Figure 6). The OPA maxima of the three compounds follows the sequence **1** < LCOOH < **2**. The molar extinction coefficients of **2** ($\varepsilon = 1.1 \times 10^5$ and 5.1×10^4 dm^3 mol^{-1} cm^{-1}) are much higher than those of LCOOH ($\varepsilon = 1.6 \times 10^4$ and 0.8×10^4 dm^3 mol^{-1} cm^{-1}) and **1** ($\varepsilon = 1.9 \times 10^4$ and 0.9×10^4 dm^3 mol^{-1} cm^{-1}); this occurs mainly as a result of the increase in the number of $LCOO^-$ units in **2**.

The OPEF spectra of all the compounds exhibit one strong emission band in CH_2Cl_2 (Figure 6). The similarities displayed in the emission bands for the complexes and LCOOH suggest their assignments as the metal-perturbed ICT of the ligand. The λ_{max}^{em} of the three compounds follows the same sequence as that of OPA, **1** < LCOOH < **2**. The OPEF intensity of **2** is much higher than those of LCOOH and **1**.

As shown in Figure 7 and Table 3, moderate redshifts are observed in the emission maxima of the three compounds in the solid state relative to the solution state. The largest redshift occurs for **1**. Such a redshift presumably arises because of the various intermolecular interactions observed

for these compounds in the solid state. The intensities of the solid-state emission bands of the two organostannoxanes are much higher than that of the ligand.

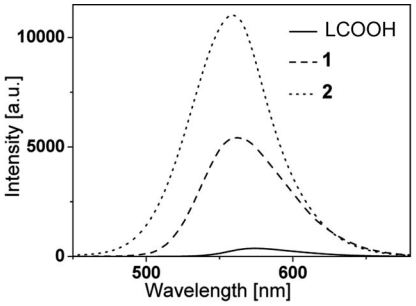

Figure 7. Solid-state luminescence spectra of LCOOH, **1**, and **2**.

Two-Photon Excited Fluorescence (TPEF) Spectroscopy and Two-Photon Absorption (TPA) Cross-Section

As shown in Figure 5a and Figure 6, above 500 nm all solutions are transparent. It is inferred that there are no molecular energy levels corresponding to a one-electron transition in this spectral range. If frequency up-converted fluorescence that is induced with a laser appears in this spectral range, it should safely be attributed to multi-photon absorption excited fluorescence. A squared dependence of the induced fluorescence power and incident laser intensity is observed, and the log plot of the fluorescence signal and excited light power provided direct evidence for two-photon excited process (Figure 8).[23]

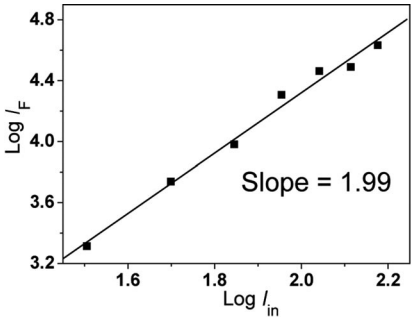

Figure 8. Linear log plot of squared dependence of the induced fluorescence signal and the incident irradiance intensity.

Detailed experiments reveal that the peak positions in the TPEF spectra of these chromophores are independent of the excitation wavelengths, but the emission intensities are dependent on the excitation wavelengths. This fact was taken into account by tuning the pump wavelengths incrementally from 720 to 860 nm, while keeping the input power fixed, and recording the TPEF intensities. Upon excitation at the optimal wavelengths, the TPEF spectra of the three compounds in CH_2Cl_2 are presented in Figure 9. The TPEF peak positions of **1** and **2** show a blueshift relative to that of LCOOH. The TPEF intensities of the three compounds follow the same sequence as that of OPEF, LCOOH < **1** < **2**.

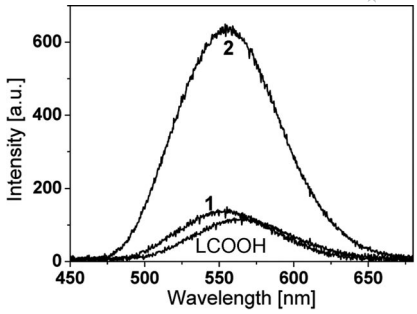

Figure 9. TPEF spectra of LCOOH, **1**, and **2** in CH_2Cl_2, under optimal excitation wavelengths.

The two-photon absorption (TPA) spectra, shown in Figure 10, were obtained by a Ti:sapphire femtosecond laser system, by the two-photon fluorescence method.[37] Under the optimal excitation wavelengths (740 nm for **1** and LCOOH, 730 nm for **2**), the δ values are 36, 53, and 223 GM for LCOOH, **1**, and **2**, respectively. It is obvious that **2** shows the best TPA property of all the three compounds and that the δ value of **2** is much higher than that of the ligand. This is mainly attributed to the increase in the number of $LCOO^-$ units in **2**. By considering the molecular weight difference between the complexes and the metal-free chromophores, the δ values for **1** and **2** were calculated to be ca. 1.5-times larger than that for LCOOH. This is because the organostannoxanes have an extended π bridge by considering the π-electron contribution from the organotin units and thus an enhanced π-electron delocalization. Moreover, the ligand has a D–π–A motif, where the metal ion binds to the acceptor rather than to the donor site, and such an arrangement should yield an increase rather than a decrease of ICT upon excitation. As a consequence, metal-ion binding is expected to result in enhanced δ values and fluorescence brightness. Thus, an increased intramolecular charge transfer may be expected in **1** and **2**, which may also account for their enhanced two-photon absorption.[38,39]

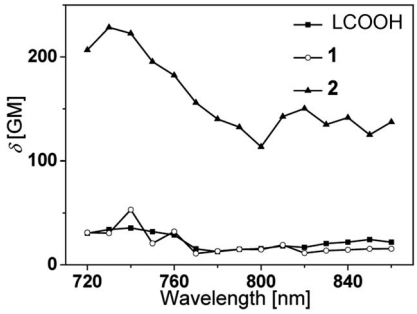

Figure 10. TPA spectra of LCOOH, **1**, and **2**.

Conclusions

A novel ligand LCOOH and two organostannoxanes have been synthesized and fully characterized. The photophysical properties have been systematically studied. All compounds possess strong fluorescence in solution upon

one- and two-photon excitation. The δ values of the two organostannoxanes are much higher than that of LCOOH, and **2** shows the best TPA property. The greater solubility of **2** in various organic solvents will facilitate the fundamental and technical applications of such organostannoxanes. It is concluded that through the stannoxane-based one-step synthetic strategy, the tetranuclear product **2** was obtained in a nearly quantitative yield, with four $LCOO^-$ units around the organooxotin cluster. The structure–property relationship studies show that the enhanced TPA response in **2** is mainly caused by the increase in the number of LCOO units and an increased ICT. Consequently, this work paves the path for the facile preparation of multi-ptz compounds that are two-photon active.

Experimental Section

Materials and Apparatus: All chemicals and solvents were dried and purified by usual methods. Elemental analysis was performed with a Perkin–Elmer 240 analyzer. IR spectra (4000–400 cm^{-1}), as KBr pellets, were recorded on a Nicolet FT–IR 170 SX spectrophotometer. Mass spectra were obtained on a Micromass GCT-MS Spectrometer. ^1H and ^{13}C NMR spectra were recorded on a Bruker AV 400 spectrometer with tms as internal standard. ^{119}Sn NMR spectra (proton-decoupled) were recorded on a Bruker AV 400 spectrometer operating at 150 MHz; resonances are referenced to tetramethyltin (external standard, ^{119}Sn).

Optical Measurements: The OPA spectra were measured on a UV-3600 spectrophotometer. The OPEF measurements were performed by using an F-2500 fluorescence spectrophotometer. The concentration of sample solution was 1.0×10^{-5} M. TPA cross-sections (δ) of the samples were obtained by the two-photon excited fluorescence (TEPF) method with a femtosecond laser pulse and a Ti:sapphire system (720–860 nm, 76 MHz, 200 fs) as the light source. The concentration of sample solution was 5.0×10^{-4} M. Thus, the δ values of samples were determined by the following Equation (1).

$$\delta_s = \delta_r \frac{F_s \cdot \Phi_r \cdot C_r \cdot n_r}{F_r \cdot \Phi_s \cdot C_s \cdot n_s} \quad (1)$$

where the subscripts "s" and "r" represent sample and reference (here, fluorescein in ethanol solution at a concentration of 1.2×10^{-4} M was used as reference), respectively. F is the overall fluorescence collection efficiency intensity of the fluorescence signal collected by the fiber spectra meter. Φ, n and c are the quantum yield of the fluorescence, the refractive index of solvent, and the concentration of the solution, respectively.

X-ray Crystallography: Single-crystal X-ray diffraction measurements were carried out on a Siemens Smart 1000 CCD diffractometer equipped with a graphite crystal monochromator situated in the incident beam for data collection at room temperature. The determination of unit cell parameters and data collections were performed with Mo-K_α radiation (λ = 0.71073 Å). Unit cell dimensions were obtained with least-squares refinements, and all structures were solved by direct methods with SHELXL-97.[40] All non-hydrogen atoms were located in successive difference Fourier syntheses. The final refinement was performed by full-matrix least-squares methods with anisotropic thermal parameters for non-hydrogen atoms on F^2. The hydrogen atoms were added theoretically and riding on the concerned atoms. The crystal data and structure refinement for the three compounds are listed in Table 4. Selected bond lengths and angles for the three compounds are summarized in Table 1 (CCDC-709735, -709736, and -709737).

Computational Details: Optimization was performed by B3LYP [6-31G(d)] without any symmetry restraints. The TDDFT {B3LYP [6-31G(d)]} calculations were then performed on the optimized structure.[34] All the calculations, including optimizations and TDDFT, were conducted with the G03 software.[35] Geometry optimization of the singlet ground state and the TDDFT calculation of the lowest 25 singlet–singlet excitation energies were calculated with a basis set composed of 6-31G* for C N O[36] and STO-3G* for H atoms, and the 6-31G* basis set for S was downloaded from the EMSL basis set library.[41] An analytical frequency analysis provides evidence that the calculated species represents a true mini-

Table 4. Crystallographic data for LCOOH, **1**, and **2**.

	LCOOH	**1**	**2**
*F*ormula	$C_{34}H_{30}N_2O_4S_2$	$C_{35}H_{29}NO_2SSn$	$C_{100}H_{128}N_4O_{10}S_4Sn_4$
M	594.16	646.34	2149.06
Crystal system	monoclinic	monoclinic	orthorhombic
Space group	$P2_1/c$	$P2_1/c$	$Pna2_1$
a [Å]	12.3422(8)	19.0846(7)	22.8922(6)
b [Å]	31.233(2)	9.3514(3)	14.2957(3)
c [Å]	7.5848(5)	16.9508(6)	31.3684(7)
α [°]	90.00	90.00	90.00
β [°]	95.855(2)	101.0710(10)	90.00
γ [°]	90.00	90.00	90.00
V [Å^3]	2908.6(3)	2968.87(18)	10265.6(4)
Z	8	4	4
D_c [g cm^{-3}]	1.358	1.446	1.391
F(000)	1248	1312	4400
Crystal Size [mm]	0.30 × 0.20 × 0.10	0.20 × 0.18 × 0.10	0.20 × 0.10 × 0.05
T [K]	298(2)	298(2)	298(2)
λ [Å]	0.71073	0.71073	0.71073
N_{ref}, N_{par}	6588, 383	6703, 362	17813, 1111
R_1, wR_2	0.0590, 0.1424	0.0297, 0.0991	0.0558, 0.0718
GOF on F^2	0.928	0.825	1.344

mum without imaginary frequencies on the respective potential energy surface. In the calculation of the optical absorption spectrum, the 25 lowest spin-allowed singlet–singlet transitions, up to an energy of ca. 5 eV, were taken into account.

(*E*)-3-(10-Ethylphenothiazin-3-yl)acrylic Acid (LCOOH): 10-Ethylphenothiazine-3-carbaldehyde (2.55 g, 0.01 mol) was heated at reflux with $CH_2(COOH)_2$ (3.12 g, 0.03 mol) and 2 drops of piperidine in pyridine (5 mL) for 3 h. The mixture was recrystallized from ethanol to afford orange crystals. Yield: 2.83 g (95%). GC/MS: *m*/*z* = 297.08 [M^+], 268.04 [$M^+ - C_2H_5$]. ^{1}H NMR (400 MHz, $CDCl_3$): δ = 1.45 (t, *J* = 7.03, 7.03 Hz, 3 H, CH_3), 3.97 (q, *J* = 6.78, 7.03, 7.03 Hz, 2 H, CH_2), 6.30 (d, *J* = 16.06 Hz, 1 H, vinyl), 6.85 (d, *J* = 8.03 Hz, 1 H), 6.89 (d, *J* = 8.28 Hz, 1 H), 6.95 (t, *J* = 7.28, 7.28 Hz, 1 H), 7.12 (d, *J* = 7.53 Hz, 1 H), 7.17 (t, *J* = 7.78, 7.78 Hz, 1 H), 7.31–7.34 (m, 2 H), 7.66 (d, *J* = 16.06 Hz, 1 H, vinyl), 12.23 (s, 1 H, COOH) ppm. ^{13}C NMR ([D$_6$]dmso): δ = 12.98, 41.80, 115.71, 116.06, 117.45, 122.59, 123.28, 123.53, 126.83, 127.51, 128.22, 128.70, 129.00, 143.27, 143.85, 146.27, 168.21 ppm. IR (KBr): $\tilde{\nu}$ = 2972 (m), 2933 (m), 2877 (m), 1686 (vs), 1594 (s), 1572 (s), 1468 (vs), 1283 (s), 1252 (s), 1204 (s), 753 (s) cm^{-1}. $C_{17}H_{15}NO_2S$ (297.37): calcd. C 68.68, H 5.05, N 4.71, O 10.78, S 10.78; found C 68.55, H 5.17, N 4.65, O 10.67, S 10.96. M.p. 214.3 °C. Orange, plate crystals of LCOOH suitable for single-crystal X-ray diffraction analysis were obtained by slow evaporation of a solution in dichloromethane/ethanol (1:1).

[Ph_3SnO_2CL] (1): $Ph_3Sn(OH)$ (0.37 g, 1 mmol) was heated at reflux with LCOOH (0.30 g, 1 mmol) in benzene (30 mL) for 8 h. The water formed in the reaction was removed by using a Dean–Stark apparatus. The reaction mixture was filtered and evaporated to afford the crude product, which was then washed with CH_2Cl_2 three times to give the yellow solid. Yield: 0.62 g (96%). ^{1}H NMR (400 MHz, [D$_6$]dmso): δ = 1.28 (t, *J* = 6.52, 6.52 Hz, 3 H, ptz-CH_2CH_3), 3.92 (q, *J* = 6.53, 6.78, 6.53 Hz, 2 H, ptz-CH_2CH_3), 6.29 (d, *J* = 16.06 Hz, 1 H, vinyl), 6.92–7.03 (m, 4 H, ptz), 7.11–7.23 (m, 4 H, ptz), 7.34–7.46 (m, 10 H, phenyl), 7.72–7.84 (d, 5 H, phenyl) ppm. ^{13}C NMR ([D$_6$]dmso): δ = 13.00, 41.73, 115.72, 116.00, 117.40, 122.69, 123.15, 123.42, 126.41, 127.50, 128.06, 128.20, 128.33, 128.67, 129.22, 129.79, 136.73, 143.11, 143.73, 144.03, 168.39 ppm. ^{119}Sn NMR ($CDCl_3$): δ = –115.6 ppm. IR (KBr): $\tilde{\nu}$ = 2981 (m), 1640 (s), 1594 (s), 1569 (s), 1468 (vs), 1404 (vs), 1349 (vs), 1222 (vs), 733 (s) cm^{-1}. $C_{35}H_{29}NO_2SSn$ (646.39): calcd. C 64.93, H 4.67, N 2.16, O 4.94, S 4.95; found C 64.87, H 4.55, N 2.28, O 4.85, S 4.80. TGA: **1** exhibits high thermal stability since there is no weight loss below 342 °C. Yellow, block crystals of **1** suitable for single-crystal X-ray diffraction analysis were obtained by slow evaporation of a petroleum ether solution.

[{[$n$$Bu_2SnO_2CL$]$_2$O}$_2$] (2): The same synthetic route as that of **1** was employed with the exception that $n$$Bu_2SnO$ (0.25 g, 1 mmol) was used, and the crude product was washed with hot petroleum ether three times to afford the yellow solid. Yield: 0.51 g (94%). ^{1}H NMR (400 MHz, [D$_6$]dmso): δ = 0.80–0.84 [m, 24 H, $(CH_2)_3CH_3$], 1.29–1.68 [m, 60 H, $(CH_2)_3CH_3$ and ptz- CH_2CH_3], 3.94 (q, *J* = 6.78, 6.78, 6.78 Hz, 8 H, ptz-CH_2CH_3), 6.94–7.04 (d, *J* = 8.28 Hz, 4 H, vinyl), 6.99 (m, 12 H, ptz), 7.14 (d, *J* = 7.28 Hz, 4 H), 7.2 (t, *J* = 7.53, 7.78 Hz, 4 H), 7.47 (m, 12 H) ppm. ^{13}C NMR ([D$_6$]dmso): δ = 7.12, 13.00, 14.07, 26.26, 27.28, 41.80, 115.76, 116.09, 116.78, 122.61, 123.28, 123.51, 126.82, 127.53, 128.26, 128.73, 129.23, 143.05, 143.93, 146.43, 168.31 ppm. ^{119}Sn NMR ($CDCl_3$): δ = –202.4, –219.2 ppm. IR (KBr): $\tilde{\nu}$ = 2954 (m), 2925 (m), 2861 (m), 1638 (s), 1596 (s), 1576 (s), 1552 (s), 1464 (vs), 1393 (vs), 1329 (vs), 1243 (vs), 747 (s) cm^{-1}. $C_{100}H_{128}N_4O_{10}S_4Sn_4$ (2149.06): calcd. C 55.84, H 5.96, N 2.61, O 7.45, S 5.96; found C 55.72, H 5.87, N 2.68, O 7.51, S 5.80. TGA: **2** also exhibits high thermal stability since there is no weight loss below 347 °C. Yellow, prismlike crystals of **2** suitable for single-crystal X-ray diffraction analysis were obtained by slow evaporation of a solution in acetone/dichloromethane/petroleum ether (1:1:1).

Acknowledgments

This work was supported by a grant for the National Natural Science Foundation of China (50532030, 20771001 and 50703001), the Team for Scientific Innovation Foundation of Anhui Province (2006KJ007TD), the Doctoral Program Foundation of the Ministry of Education of China, Education Committee of Anhui Province (KJ2009A52).

[1] Y. P. Tian, L. Li, J. Z. Zhang, J. X. Yang, H. P. Zhou, J. Y. Wu, P. P. Sun, L. M. Tao, Y. H. Guo, C. K. Wang, H. Xing, W. H. Huang, X. T. Tao, M. H. Jiang, *J. Mater. Chem.* **2007**, *17*, 3646–3654.
[2] G. S. He, J. Swiatkiewicz, Y. Jiang, P. N. Prasad, B. A. Reinhardt, L. S. Tan, R. Kannan, *J. Phys. Chem. A* **2000**, *104*, 4805–4810.
[3] S. Sivakumar, F. C. J. M van Veggel, P. S. May, *J. Am. Chem. Soc.* **2007**, *129*, 620–625.
[4] H. M. Kim, M. S. Seo, M. J. An, J. H. Hong, Y. S. Tian, J. H. Choi, O. Kwon, K. J. Lee, B. R. Cho, *Angew. Chem. Int. Ed.* **2008**, *47*, 5167–5170.
[5] I. Roy, T. Y. Ohulchanskyy, H. E. Pudavar, E. J. Bergey, A. R. Oseroff, J. Morgan, T. J. Dougherty, P. N. Prasad, *J. Am. Chem. Soc.* **2003**, *125*, 7860–7865.
[6] C. Wu, C. Szymanski, Z. Cain, J. McNeill, *J. Am. Chem. Soc.* **2007**, *129*, 12904–12905.
[7] A. Bhaskar, G. Ramakrishna, Z. Lu, R. Twieg, J. M. Hales, D. J. Hagan, E. V. Stryland, T. Goodson, *J. Am. Chem. Soc.* **2006**, *128*, 11840–11849.
[8] N. J. Durr, T. Larson, D. K. Smith, B. A. Korgel, K. Sokolov, A. Ben-Yakar, *Nano Lett.* **2007**, *7*, 941–945.
[9] A. M. McDonagh, M. G. Humphrey, M. Samoc, B. Luther-Davies, *Organometallics* **1999**, *18*, 5195–5197.
[10] M. Gielen, A. G. Davies, K. Pannell, E. Tiekink, *Tin Chemistry: Fundamentals, Frontiers, and Applications*, VCH, Weinheim, **2008**, p. 413.
[11] R. R. Holmes, C. G. Schmid, V. Chandrasekhar, R. O. Day, J. M. Holmes, *J. Am. Chem. Soc.* **1987**, *109*, 1408–1414.
[12] V. Chandrasekhar, S. Nagendran, S. Bansal, M. A. Kozee, D. R. Powell, *Angew. Chem. Int. Ed.* **2000**, *39*, 1833–1836.
[13] R. O. Day, J. M. Holmes, V. Chandrasekhar, R. R. Holmes, *J. Am. Chem. Soc.* **1987**, *109*, 940–941.
[14] K. C. Kumara Swamy, R. O. Day, R. R. Holmes, *J. Am. Chem. Soc.* **1987**, *109*, 5546–5548.
[15] V. Chandrasekhar, R. O. Day, J. M. Holmes, R. R. Holmes, *Inorg. Chem.* **1988**, *27*, 958–966.
[16] D. Dakternieks, K. Jurkschat, D. Schollmeyer, H. Wu, *Organometallics* **1994**, *13*, 4121–4123.
[17] M. Mehring, M. Schürmann, H. Reuter, D. Dakternieks, K. Jurkschat, *Angew. Chem. Int. Ed. Engl.* **1997**, *36*, 1112–1114.
[18] C. García, R. Oyola, L. E. Piñero, R. Arce, J. Silva, V. Sánchez, *J. Phys. Chem. A* **2005**, *109*, 3360–3371.
[19] M. Hauck, J. Schönhaber, A. J. Zucchero, K. I. Hardcastle, T. J. J. Müller, U. H. F. Bunz, *J. Org. Chem.* **2007**, *72*, 6714–6725.
[20] S. Nath, H. Pal, D. K. Palit, A. V. Sapre, J. P. Mittal, *J. Phys. Chem. A* **1998**, *102*, 5822–5830.
[21] D. G. Nocera, H. B. Gray, *J. Am. Chem. Soc.* **1981**, *103*, 7349–7350.
[22] G. W. Kim, M. J. Cho, Y. J. Yu, Z. H. Kim, J.-I. Jin, D. Y. Kim, D. H. Choi, *Chem. Mater.* **2007**, *19*, 42–50.

[23] Y. P. Tian, M. L. Zhang, X. Q. Yu, G. B. Xu, Y. Ren, J. X. Yang, J. Y. Wu, X. J. Zhang, X. T. Tao, S. Y. Zhang, M. H. Jiang, *Chem. Phys. Lett.* **2004**, *388*, 325–329.
[24] R. R. Holmes, *Acc. Chem. Res.* **1989**, *22*, 190–197.
[25] E. R. T. Tiekink, *Appl. Organomet. Chem.* **1991**, *5*, 1–23.
[26] V. K. Jain, *Coord. Chem. Rev.* **1994**, *135*, 809–843.
[27] V. Chandrasekhar, S. Nagendran, V. Baskar, *Coord. Chem. Rev.* **2002**, *235*, 1–52.
[28] a) G. Wu, X. F. Wang, T. Okamura, W. Y. Sun, N. Ueyama, *Inorg. Chem.* **2006**, *45*, 8523–8532; b) B. H. Ye, M. L. Tong, X. M. Chen, *Coord. Chem. Rev.* **2005**, *249*, 545–565.
[29] W. Lu, Z. M. Yan, J. Dai, Y. Zhang, Q. Y. Zhu, D. X. Jian, W. J. Guo, *Eur. J. Inorg. Chem.* **2005**, 2339–2345.
[30] a) H. F. Zhu, J. Fan, T. Okamura, Z. H. Zhang, G. X. Liu, K. B. Yu, W. Y. Sun, N. Ueyama, *Inorg. Chem.* **2006**, *45*, 3941–3948; b) S. B. Suh, J. C. Kim, Y. C. Choi, S. Yun, K. S. Kim, *J. Am. Chem. Soc.* **2004**, *126*, 2186–2193; c) B. Q. Ma, H. L. Sun, S. Gao, *Angew. Chem. Int. Ed.* **2004**, *43*, 1374–1376.
[31] V. Chandrasekhar, P. Thilagar, A. Steiner, J. F. Bickley, *Chem. Eur. J.* **2006**, *12*, 8847–8861.
[32] a) G. R. Desiraju, *Acc. Chem. Res.* **1996**, *29*, 441–449; b) V. Chandrasekhar, K. Gopal, S. Nagendran, *Cryst. Growth Des.* **2006**, *6*, 267–273.
[33] a) B. G. Zhang, J. Xu, Y. G. Zhao, C. Y. Duan, X. Cao, Q. J. Meng, *Dalton Trans.* **2006**, 1271–1276; b) G. R. Desiraju, *Acc. Chem. Res.* **2002**, *35*, 565–573.
[34] L. Yang, J. K. Feng, A. M. Ren, *J. Org. Chem.* **2005**, *70*, 5987–5996.
[35] M. J. Frisch, G. W. Trucks, H. B. Schlegel, G. E. Scuseria, M. A. Robb, J. R. Cheeseman, J. A. Montgomery Jr, T. Vreven, K. N. Kudin, J. C. Burant, J. M. Millam, S. S. Iyengar, J. Tomasi, V. Barone, B. Mennucci, M. Cossi, G. Scalmani, N. Rega, G. A. Petersson, H. Nakatsuji, M. Hada, M. Ehara, K. Toyota, R. Fukuda, J. Hasegawa, M. Ishida, T. Nakajima, Y. Honda, O. Kitao, H. Nakai, M. Klene, X. Li, J. E. Knox, H. P. Hratchian, J. B. Cross, C. Adamo, J. Jaramillo, R. Gomperts, R. E. Stratmann, O. Yazyev, A. J. Austin, R. Cammi, C. Pomelli, J. W. Ochterski, P. Y. Ayala, K. Morokuma, G. A. Voth, P. Salvador, J. J. Dannenberg, V. G. Zakrzewski, S. Dapprich, A. D. Daniels, M. C. Strain, O. Farkas, D. K. Malick, A. D. Rabuck, K. Raghavachari, J. B. Foresman, J. V. Ortiz, Q. Cui, A. G. Baboul, S. Clifford, J. Cioslowski, B. B. Stefanov, G. Liu, A. Liashenko, P. Piskorz, I. Komaromi, R. L. Martin, D. J. Fox, T. Keith, M. A. Al-Laham, C. Y. Peng, A. Nanayakkara, M. Challacombe, P. M. W. Gill, B. Johnson, W. Chen, M. W. Wong, C. Gonzalez, J. A. Pople, *Gaussian 03*, Revision B.04, Gaussian, Inc., Pittsburgh, PA, **2003**.
[36] F. D. Angelis, S. Fantacci, A. Sgamellotti, E. Cariati, R. Ugo, P. C. Ford, *Inorg. Chem.* **2006**, *45*, 10576–10584.
[37] C. Xu, W. W. Webb, *J. Opt. Soc. Am. B (Optical. Physics)* **1996**, *13*, 481–491.
[38] Q. Zheng, G. S. He, P. N. Prasad, *J. Mater. Chem.* **2005**, *15*, 579–587.
[39] S. Sumalekshmy, M. M. Henary, N. Siegel, P. V. Lawson, Y. Wu, K. Schmidt, J. L. Brédas, J. W. Perry, C. J. Fahrni, *J. Am. Chem. Soc.* **2007**, *129*, 11888–11889.
[40] G. M. Sheldrick, *SHELXL-97: Program for Crystal Structure Refinement*, University of Göttingen, Göttingen, Germany, **1997**.
[41] EMSL basis set library available at http://www.emsl.pnl.gov/forms/basisform.html.

Received: March 6, 2009
Published Online: May 13, 2009

